Photonic applications of spatial photorefractive solitons - soliton lattices, bidirectional waveguides and waveguide couplers

Cornelia Denz, Anton Desyatnikov, Philip Jander, Jochen Schröder, Denis Träger
Institut für Angewandte Physik, Westfälische Wilhelms-Universität Münster,
Corrensstr. 2-4, D 48149 Münster, Germany
Milivoj Belic, Milan Petrovic, Aleksandra Strinic
Institute of Physics, P.O. Box 57,
11001 Belgrade, Yugoslavia
Jürgen Petter
Institut für Angewandte Physik, Technische Universität Darmstadt,
Hochschulstr. 6, D - 64289 Darmstadt, Germany
denz@uni-muenster.de

Abstract: We demonstrate the generation of large two-dimensional soliton lattices and investigate their waveguiding properties for red and infrared wavelengths. The control of these lattices is demonstrated, exploiting coherent and incoherent soliton interaction features. For applications in bidirectional waveguiding, which is of interest in self-adjustment of photonic devices, we investigate the formation of spatial solitons by counterpropagating beams, including colliding coherent solitons and bidirectional vector-solitons. The question of stability of these different configurations is addressed and dynamic scenarios are reported.
OCIS codes: 190.0190 (General); 190.4420 (Nonlinear optics, transverse effects in); 190.5330 (Photorefractive nonlinear optics); 190.5940 (Self-action effects); 190.5530 (Pulse propagation and solitons).

Introduction

Adaptive waveguides are of particular interest in all-optical information processing due to their potential to realize large arrays as well as many configurations that allow different interconnection schemes. Optical spatial solitons have been proposed for these applications owing to their ability to guide waves and their interaction capabilities, and demonstrations as waveguides [1], as directional couplers [2], light-induced Y and X-couplers and beam splitters [3] have proven this potential. In addition to these one- or two waveguide configurations, which involve only a limited number of spatial solitons, the parallel propagation of several spatial solitons – so-called soliton pixels, soliton arrays or soliton lattices – have been suggested for applications in information processing [4,5]. Recently, several demonstrations showed that large arrays of spatial solitons can be formed in parametric amplifiers [6] or in photorefractive media for coherent [7,8], and incoherent solitons [9]. Moreover, they have been suggested for image reconstruction applications [7,10].
In this contribution, we combine the features of spatial photorefractive solitons to form stable constituents during interaction and large pixel-like lattices with waveguiding features. Thereby, we realize waveguiding in large arrays of soliton lattices at red and infrared wavelengths, and achieve control of these lattices by phase-dependent interactions for both, copropagating and counterpropagating solitons. Most interaction configurations have been realized up to now between solitons that co-propagate in the nonlinear material. After having been investigated theoretically already some time ago [11], it was only recently that counterpropagating beams have been considered in photorefractive materials for the case of one transverse

dimension [12,13]. However, configurations of counter-propagation are of high application potential in bidirectional, self-adjustable interconnections of arrays of waveguides. Here, we demonstrate the formation and interaction of complex arrays of solitons in the counter-propagation geometry for coherent interactions.

Lattices of spatial solitons

To create large two-dimensional lattices of photorefractive solitons, the conditions for stable and non-interacting propagation need to be defined. A crucial point in the parallel propagation of photorefractive spatial solitons is their anisotropic mutual interaction [14]. Because the refractive index modulation induced by each single soliton reaches beyond its effective waveguide, phase-dependent coherent as well as separation-dependent incoherent interactions as repulsion, attraction or fusion may appear between neighbouring array elements [15]. These interaction effects also affect the waveguiding features in a soliton channel. Therefore, the parallel propagation of a multitude of solitons can only be achieved if the separation is carefully chosen in such a way to minimize all forms of interactions. In our experiments, we determined the critical soliton distance, at which interaction occurs and fixed the distance to a value that is beyond this limit.

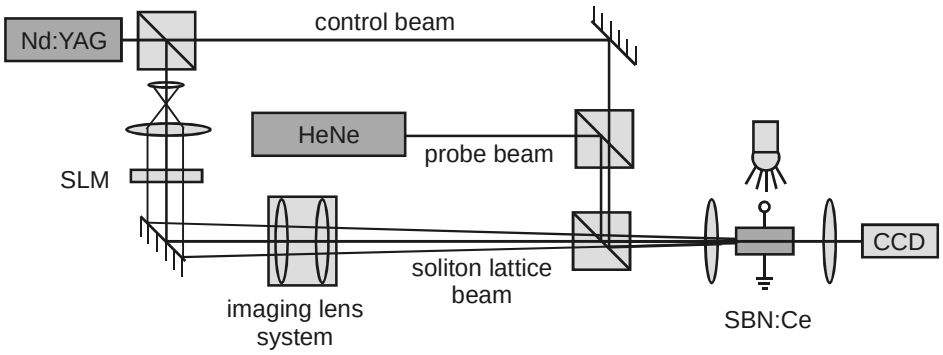

Fig. 1: Schematic setup for the creation, waveguiding and control of large lattices of photorefractive screening solitons.

To create lattices of solitons in a photorefractive crystal, the typical setup of soliton formation was modified in such a way that the laser beam derived from a frequency-doubled Nd:YAG-laser emitting at λ = 532 nm illuminates a spatial light modulator which imprints the image of a spot array onto the beam (see fig. 1). The spatial light modulator in turn is imaged onto the front face of a photorefractive SBN60:Ce crystal (5 x 5 x 20 mm^3, with the propagation direction along the 20 mm axis as in typical soliton formation experiments). In order to exploit the dominant electro-optic coefficient r_{33} of our SBN probe, the incident

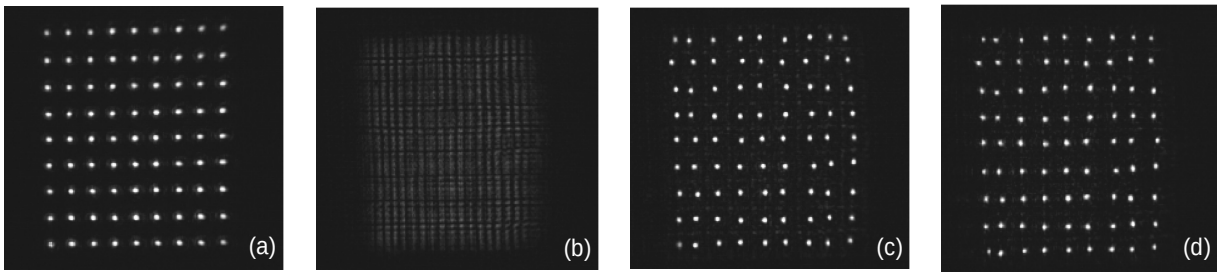

Fig. 2: Realization of a 9 x 9 spatial soliton lattice. a) Front face of the photorefractive SBN-crystal (image of the spot array created by a spatial light modulator, b) interference pattern due to linear propagation at the exit face of the crystal, c) and d) array of 81 spatial solitons at the exit face of the crystal after 5 and 30 min of formation, respectively.

laser beam was linearly polarized parallel to the c-axis of the crystal. For the creation of soliton lattices and testing of its waveguiding properties, regular patterns of up to 25 x 25 spots each with a diameter of about 20 μm and an intensity of about 110 nW are imaged onto the front face of the crystal (Fig. 2a). In the linear case - without applied electric field - the beams diffract on their way through the crystal and display a typical interference pattern (Fig. 2b). Applying an external electric field of about 1 kV/cm and using a supplementary white light source to create an artificial dark conductivity in such a way to achieve spatial photorefractive screening soliton formation, self-focusing forms lattices of solitons (Fig. 2c).
To obtain propagation without mutual interaction, we take care that the initial distance between single solitons is just large enough to prevent soliton interactions. Therefore, the horizontal and vertical initial separations are chosen to be $\Delta x = 100$ μm and $\Delta y = 124$ μm. Slight deviations from the symmetry are due to inhomogeneities of the crystal. A distance smaller than the critical distance for coherent interactions between the solitons in either case would cause the solitons to interact and eventually fuse due to their own mutual attractive force. Such a situation is shown in Fig. 3, where the distance was reduced by enhancing the number of solitons in the same transverse area.

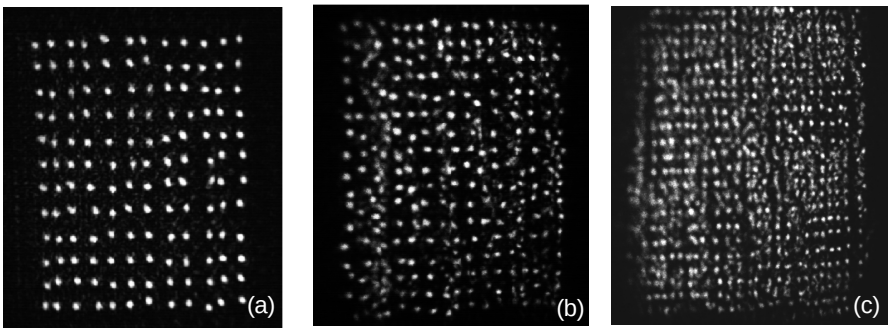

Fig. 3: Interaction of solitons in large lattices for distances smaller than the critical distance of independent propagation. a) 12 x 12 solitons, with $\Delta x = 70$ μm, $\Delta y = 85$ μm, b) 17 x 17 solitons, $\Delta x = 60$ μm, $\Delta y = 75$μm, c) 25 x 25 solitons, $\Delta x = 50$ μm, $\Delta y = 65$ μm (all values ± 3 μm due to pixel mismatch between input configurations and the SLM device).

In our numerical simulations based on the paraxial approximation to the propagation of an optical beam in an anisotropic saturable medium, a similar behaviour was found: parallel propagation of solitons with a given mutual distance can be adjusted to be almost without interaction (Figs. 4a, 4b), whereas separations below the critical lengths lead to fusion of columns of beams (Figs. 4c, 4d) in the array. In order to achieve a closer package in such a soliton array while maintaining propagation without interaction, the phase

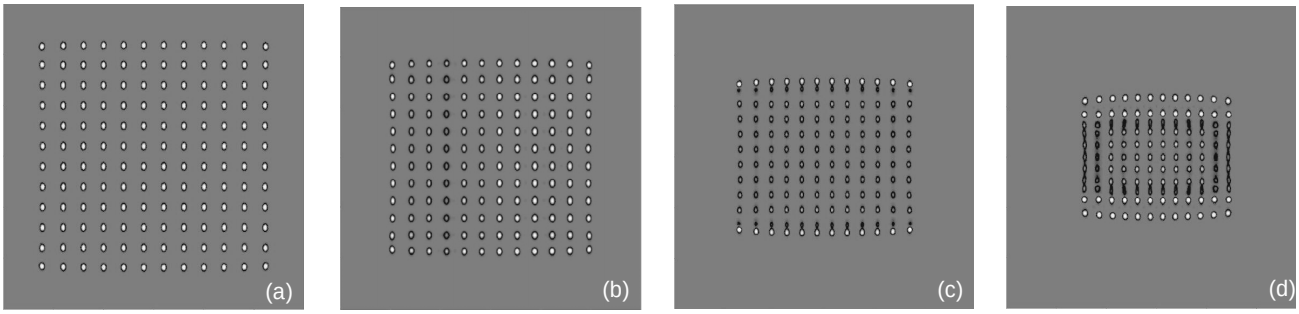

Fig. 4: Numerical simulation of large soliton lattices for z = 35 mm of propagation, an electric field of 900 V/cm with an effective electrooptic coefficient of 210 pm/V, and an initial mutual distance at z = 0 of a) $\Delta x = \Delta y = 80$ μm, b) $\Delta x = \Delta y =$ 70 μm, c) $\Delta x = \Delta y = 60$ μm, d)) $\Delta x = \Delta y = 50$ μm.

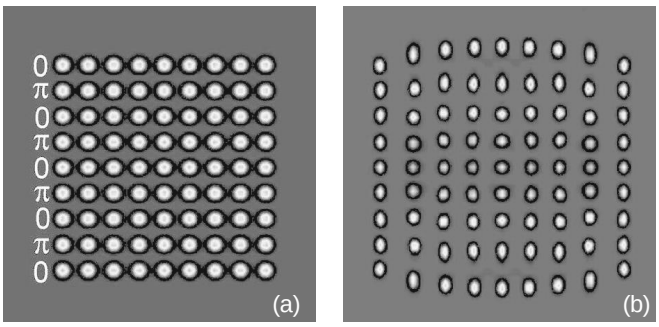

Fig. 5: Stabilization of soliton lattices by phase engineering of the relative phases of the beams. a) Phase relationship at the entrance face of the nonlinear material ($\Delta x = \Delta y = 35\mu m$). b) Soliton lattice for z = 35 mm propagation (E =1,3 kV/cm).

relationship between different beams of the array can be exploited. By engineering the relative phases between different rows of beams to alternate between 0 and π at the entrance face of the material, a propagation with reduced interaction can be stabilized. Fig. 5 shows a situation for a larger electric field and a smaller separation distance between solitons in the lattice. However, the resulting interaction is lower due to the phase relationship between neighbouring solitons that prevents interaction.

Waveguiding in soliton lattices

To test for the waveguide properties of the single channels of such a soliton array, the wavelength selectivity of the photorefractive effect in our SBN:Ce probe [16] is exploited to scan the soliton array with an intense probe beam without significantly destroying single soliton channels. The wavelength of the probe beam was either λ = 633 nm or λ = 1550 nm. Positioning the red or infrared probe beam successively to the positions of the previously induced solitons on the crystals front face, we find the probe beam to be guided in each of the soliton channels solely. Scans of this array with the red or infrared probe beam are shown in Fig. 6. To obtain information of the complete array, every single channel is scanned separately, and the individual images are superimposed electronically. Infrared beams have been visualized using an infrared converter system [17].

Naturally, larger arrays of solitons can also be formed. Their number is mainly limited by the aperture of the photorefractive crystal and the resolution of the inducing spatial light modulator. Examples of different soliton lattices that can be achieved are shown in fig. 7, where the distances between neighbouring solitons where chosen to ensure non interacting solitons. In larger arrays, several applications of parallel soliton and waveguide formation can be considered. As an example, digitized images consist of large arrays of pixellike spots arranged on a square lattice. In the linear regime, such an image can be reconstructed only in a range that is limited by the depth of focus of the imaging optics due to the blurring effects of diffraction.

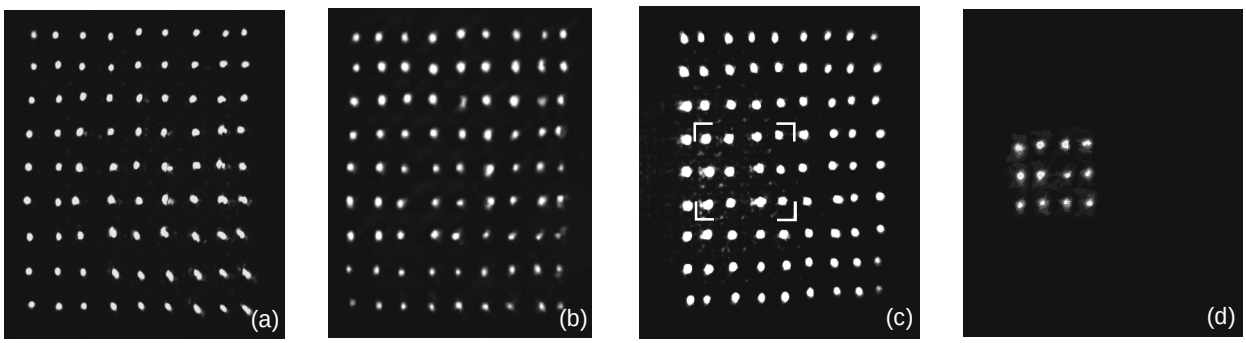

Fig. 6: Probing a soliton array by waveguiding a probe beam of a different wavelength in the individual soliton channel. a) soliton array formed at λ = 532 nm, b) probing the array with λ = 633 nm in individual soliton channels, c) soliton array formed at λ = 532 nm, d) probing a part of the array with λ = 1550 nm, visualized with an infrared-to-visible light converter [17]. The results are electronically added to show waveguiding of numerous solitons in the array simultaneously.

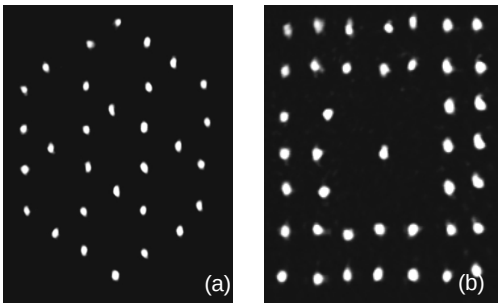

Fig. 7: Examples of different configurations of photonic lattices induced by spatial photorefractive solitons. a) Hexagonal lattice with holes, b) square lattice with a row left out.

However, if these arrays of spots are propagating in a nonlinear, solitonic regime, we are able to enlarge the range of focus depth to the length of the soliton formation, i.e. to the length of the nonlinear crystal. This idea [10] has also been demonstrated in our system with a regular pattern of 25 spots [8].

Interaction in soliton lattices

To use these soliton arrays for applications in information technology, it is highly desirable to have means of manipulating individual waveguides in order to combine different channels, separate them or induce energy exchange between them. For this purpose, well-known interaction scenarios of spatial photorefractive solitons can be exploited. Two different principles can be employed to induce these interactions in large soliton arrays. In the first approach, another beam can be created in the SLM configuration between the regular spots of the soliton array, thereby forming a soliton that has a relative distance to neighbouring solitons below the critical distance. Varying the phase of this soliton by changing the SLM steering voltage, phase-sensitive coherent or incoherent interaction that may lead to fusion or repulsion of different solitons can be realized. In a second approach which we utilize here, a supplementary control beam derived from the Nd:YAG-laser is focused onto the front face of the SBN crystal. While in this experiment the array solitons had an intensity of 55 mW/cm^2 each, the separate controlling beam, which was positioned between two spots of the array, had an intensity of about 160 mW/cm^2. In fig. 8, the back face of the crystal with the uncontrolled array is shown. Once the control beam was positioned between the central lower two solitons and the electric field was applied the new soliton array formed. Due to the additional beam between the two lower central channels, the refractive index in between these channels is increased causing the two solitons to attract and eventually fuse. Fig. 8b shows the red probe beam guided in each channel of the controlled array separately (again single snapshots were added electronically). Here, the fusion of the two lower middle channels is obvious. Therefore, the case of coupling the probe beam into the central or the lower middle channel on the front face of the crystal leads to guiding it into the same output, respectively.

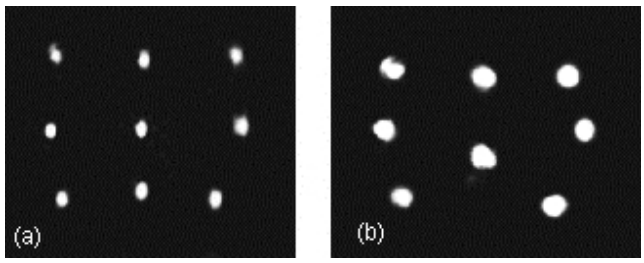

Fig. 8: Optical control of soliton lattices. a) Uncontrolled lattice, b) controlled lattice probed at λ = 633 nm. The slight size mismatch of both figures is due to wavelength dependence of aberrations in the imaging system.

Counterpropagating solitons

So far, the formation and interaction of photorefractive screening solitons have been studied mainly in the co-propagation geometry. However, due to the application potential of counterpropagating soliton lattices as beam couplers, interest in experimental realizations of this configuration has grown recently [12,13]. Here, we develop a numerical description of the counterpropagating soliton configuration for one transverse dimension, taking into account the periodic modulation of the space field induced by the interference of the counterpropagating beams. The interaction of the two beams, which includes feedback and dynamical effects, makes counterpropagating solitons different from their copropagating

counterparts. Therefore, the resulting space charge field consists of two components, an unmodulated part E_0 of the transverse component and a modulated part E_1, which is proportional to the modulation depth m of the interference of both beams having the wave vector k. In order to describe the impact of these fields on the beam propagation, we formulate the space charge field in a normalized way relative to the externally applied electric field E_{ext}

$$E_{sc} = E_0 + 0.5\left(E_1 \exp(-2ikz) + c.c.\right) \tag{1}$$

Assuming a local, isotropic approximation of the space charge field and a saturable nonlinearity $E_{sc} = 1/(1+I)$ with I being the light intensity normalized relative to the background intensity, the temporal evolution of the space charge field is introduced assuming a relaxation-type dynamics

$$\tau\partial_t E_0 + E_0 = -I_0/(1+I_0), \qquad \tau\partial_t E_1 + E_1 = -\varepsilon m/(1+I_0) \tag{2}$$

with $I_0 = |F|^2 + |B|^2$ and $m = 2FB^*/(1+I_0)$, and the relaxation time τ of the crystal being inversely proportional to the total intensity. ε describes the relative coherence of the forward and the backward propagating beams, i.e. $\varepsilon = 0$ for incoherent and $\varepsilon = 1$ for coherent interaction. Inserting these conditions in the paraxial wave equation leads to the propagation equations for the forward (F) and backward (B) propagating beams. In the normalized form, setting $x \rightarrow x/x_0$, $z \rightarrow z/L_D$, $(F,B) \rightarrow (F,B)\exp(-i\Gamma z)$ with the diffraction length $L_D = 2kx_0^2$, and denoting the constant $(kn_0x_0)^2 r_{eff} E_{ext}$ by Γ, where n_0 is the refractive index of the nonlinear material, x_0 is the transverse beam waist, and r_{eff} is the electro-optic coefficient, the propagation equations are given by

$$\begin{aligned} +i\partial_z F + \partial_x^2 F &= \Gamma(E_0 F + E_1 B/2) \\ -i\partial_z B + \partial_x^2 B &= \Gamma(E_0 B + E_1^* F/2). \end{aligned} \tag{3}$$

Solving these equations numerically, we find localized structures that are stationary in time and represent self-trapped waveguides. Fig. 9 shows the counter-propagation of two coherent Gaussian beams that are launched at different lateral positions. When the initial separation is less than four beam diameters, the individual solitons begin to interact. For a separation about two beam diameters, the interaction is strong enough for the beams to form a single waveguiding structure. Head-on collisions result in the formation of a counterpropagating vector-soliton as was shown in [12].

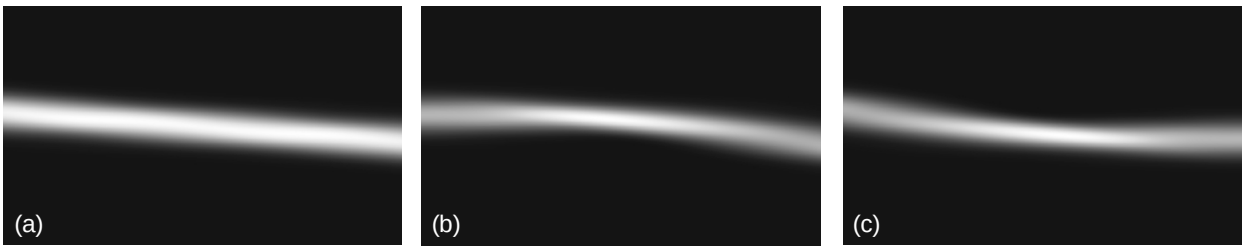

Fig. 9: Counterpropagating self-trapped waveguide formed out of two coherent beams. a) Resulting spatial intensity distribution in steady state, b) right-propagating beam, c) left-propagating beam. The size of the data windows is 10 beam diameters in the transverse direction and two diffraction lengths in the direction of beam propagation. The initial integrated intensities are $|F|^2 = |B|^2 = 1$, the coupling strength is $\Gamma = 5$.

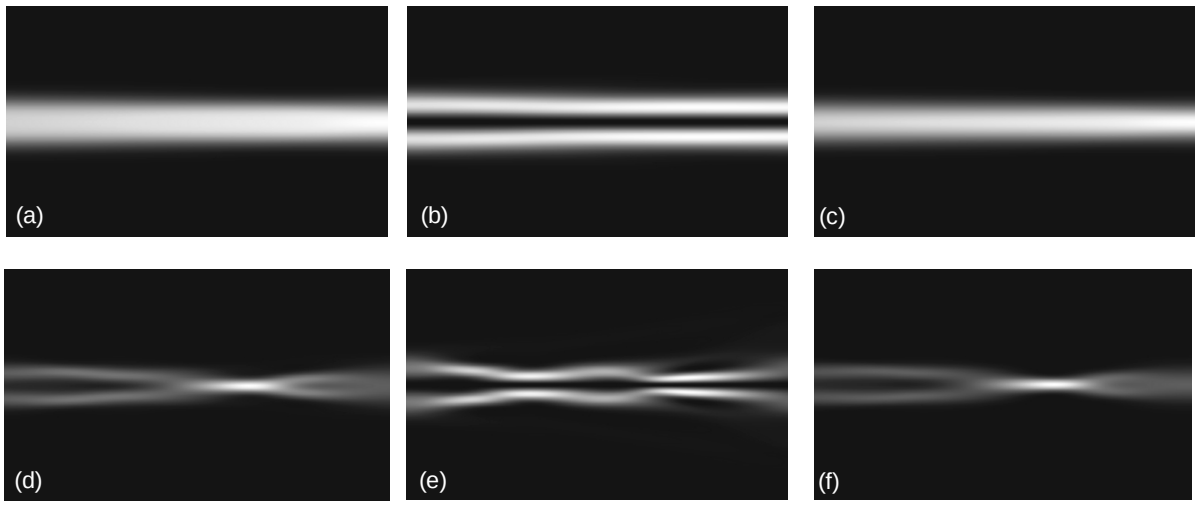

Fig. 10: Intensity distribution of counterpropagating localized structures (a,d), created by the interaction of a right-propagating dipole-mode beam (b,e) and a left-propagating soliton (c,f). In the top row, a counterpropagating dipole-mode vector soliton is formed ($\Gamma = 3{,}3$) (a), whereas in the bottom row a modulation instability develops ($\Gamma = 12$) and forms self-trapped waveguides (d). All other data as in Fig. 9.

The generation of a photorefractive dipole-mode counterpropagating vector soliton is presented in Fig. 10 (a-c). A dipole beam is launched from the left, and a power-matched, coherent single beam from the right. Such a bimodal counterpropagating soliton has already been theoretically predicted and found to be stable for Kerr nonlinearities [11,18]. If photorefractive nonlinearity in such a configuration is above a certain threshold, modulation instabilities in the longitudinal direction prevent soliton formation, leading to stationary localized structures. Fig. 10 (d-f) shows an example of such a situation with the same initial beams as in fig. 10 (a-c), but with a coupling strength that is around four times larger than before.

Counterpropagating solitons also may form self-trapped structures that dynamically do not converge to a steady-state, especially when complex spatial structures counter-propagate for high nonlinearities. Fig. 11 shows a situation where three in-phase beams propagate to the right, and two out-of-phase beams propagate to the left. Such a configuration represents a novel time- as well as z-dependent complex localized structure that can not be described by the usual steady-state theory of spatial solitons. Its z-dependence can be attributed to the general features of longitudinal waveguides, whereas the time-dependence is governed by the slow response of the photorefractive medium.

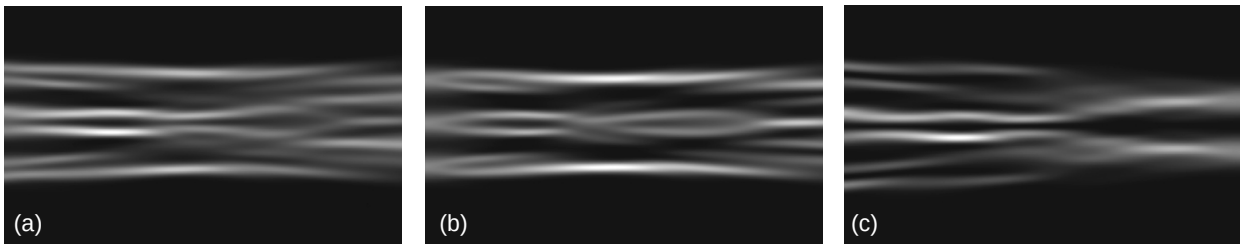

Fig. 11: Unstable self-organized localized structure resulting after 116 time steps (a): three in-phase beams (b) entering the material from the left counterpropagate with two out-of phase beams propagating from right to left (c). The total power that enters to the left and to the right are equal, the coupling constant is given by $\Gamma = 10$. All other data as in fig. 9.

Conclusion

To summarize, we have discussed several aspects of interaction of multiple solitons for applications in all-optical waveguiding and interconnects. We have presented the formation of large two-dimensional lattices of solitons that are able to guide light at different wavelengths. Moreover, a control of these channels is possible by exploiting different interaction features of coherent and incoherent photorefractive solitons. We have shown how to use a supplementary steering beam in order to fuse selected solitons in the soliton lattice. In the counterpropagating soliton geometry, the inclusion of time-dependent effects is crucial for understanding the formation of waveguide structures. We demonstrated by our numerical analysis the generation of a counterpropagating vector soliton, and presented a novel class of localized, non-solitonic stationary solutions. Moreover, dynamical states and the onset of longitudinal modulational instabilities were depicted. Experimental investigations to exploit these novel states and dynamical scenarios are currently in progress.

Acknowledgements

Part of this work was supported by the Graduiertenkolleg “Nichtlineare kontinuierliche Systeme” of the Deutsche Forschungsgemeinschaft. MB, AS, and AD gratefully acknowledge support from the Alexander von Humboldt-Stiftung, DT acknowledges support from the Konrad-Adenauer-Stiftung. We are also indebted to H.-G. Purwins and S. Matern for support in visualizing waveguiding at infrared wavelength with an infrared-conversion system [17].

References

1. M. Shih, Z. Chen, M. Mitchell, M. Segev, et al., J. Opt. Soc. Am. B 14 3091 (1997).
2. S. Lan, E. DelRe, Z. Chen, M. Shih, M. Segev, Opt. Lett. 24 475 (1999).
3. J. Petter, C. Denz, Opt. Comm. 188 55 (2001).
4. P.V. Mamyshev, C. Bosshard, G.I. Stegeman, J. Opt. Soc. Am. B 11 1254 (1994).
5. W. Krolikowski, Yu.S. Kivshar, Journ. Opt. Soc. Am. B 13 24 (1996).
6. S. Minardi, S. Sapone, W. Chinaglia, P. Di Trapani, A. Berzanskis, Opt. Lett. 25 326 (2000).
7. C. Weilnau, M. Ahles, J. Petter, D. Träger, J. Schröder, C. Denz, Annalen der Physik 9 1 (2002).
8. J. Petter, J. Schröder, D. Träger, C. Denz, Opt. Lett. 28 438 (2003).
9. Z. Chen, K. McCarthy, Opt. Lett. 27 2019 (2002).
10. A. Bramati, W. Chinaglia, S. Minardi, P. Di Trapani, Opt. Lett. 26 1409 (2001).
11. M. Haelterman, A.P. Sheppard, A.W. Snyder, Opt. Commun. 103 145 (1993).
12. O. Cohen, R. Uzdin, T. Carmon, J. W. Fleischer, M. Segev, S. Odoulov, Phys. Rev. Lett. 89 13 (2002).
13. O. Cohen, S. Lan, T. Carmon, J.A. Giordmaine, M. Segev, Opt. Lett. 15 22 (2002).
14. W. Krolikowski, M. Saffman, B. Luther-Davies, C. Denz, Phys. Rev. Lett. 80 3240 (1998).
15. W. Krolikowski, C. Denz, A. Stepken, M. Saffman, B. Luther-Davies, Quant. Semiclass. Opt. 10 823 (1998).
16. J. Petter, C. Denz, Journ. Opt. Soc. Am. B. 19 1145 (2002).
17. S. Matern, V.M. Marchenko, Yu.A. Astrov, L.M. Portsel, H.-G. Purwins, Proc.SPIE 4669 13 (2002).
18. E.A. Ostrovskaya, Y.S. Kivshar, D.V. Skryabin, W.J. Firth, Phys. Rev. Lett. 83 296 (1999).